Transgenic mouse models in migraine

Ven, R.C.G. van de

CHAPTER 2

TWO

R192Q knockin migraine mouse model: increased susceptibility to cortical spreading depression and cerebellar MRI abnormalities

Chapter 2A

A *Cacna1a* knockin mouse model with increased susceptibility to cortical spreading depression

A.M.J.M. van den Maagdenberg,[1,2]* D. Pietrobon,[3]* T. Pizzorusso,[4] S Kaja,[2,5] L.A.M. Broos,[1] T. Cesetti,[3] R.C.G. van de Ven,[1] A. Tottene,[3] J. van der Kaa,[1] J.J. Plomp,[2,5] R.R. Frants,[1] M.D. Ferrari[2]

*Authors contributed equally

Department of [1]Human Genetics, [2]Neurology and [5]Neurophysiology, Leiden University Medical Centre, Leiden, The Netherlands

[3]Department of Biomedical Sciences, University of Padova, Padova, Italy

[4]Scuola Normale Superiore, Istituto Neuroscienze CNR, Pisa, Italy

Neuron, 41 (2004) p. 701-710

Summary

Migraine is a common, disabling, multifactorial, episodic neurovascular disorder of unknown etiology. Familial hemiplegic migraine type 1 (FHM-1) is a Mendelian subtype of migraine with aura that is caused by missense mutations in the *CACNA1A* gene that encodes the α_1-subunit of neuronal $Ca_v2.1$ Ca^{2+} channels. We generated a knockin mouse model carrying the human pure FHM-1 R192Q mutation and found multiple *gain-of-function* effects. These include increased $Ca_v2.1$ current density in cerebellar neurons, enhanced neurotransmission at the neuromuscular junction and, in the intact animal, a reduced threshold and increased velocity of cortical spreading depression (CSD; the likely mechanism for the migraine aura). Our data show that the increased susceptibility for CSD and aura in migraine may be due to cortical hyperexcitability. The R192Q FHM-1 mouse is a promising animal model to study migraine mechanisms and treatments.

Introduction

Migraine is a common, chronic neurovascular disorder, typically characterized by recurrent attacks (1-3 days) of disabling headaches and associated autonomic symptoms. In one-third of patients, attacks are accompanied by transient neurological aura symptoms.[1] Twelve percent of the general population have on average 1-2 migraine attacks per month and WHO rates migraine in the highest class of most disabling chronic disorders; treatments are frequently unsatisfactory.[1]

The etiology of migraine is multifactorial (for reviews see[1,2]). The migraine pain is likely to be caused by activation of the trigeminovascular system, which primarily consists of trigeminal afferents innervating meningeal bloodvessels, the trigeminal nerve, and brainstem nuclei that modulate sensory signal transmission. Neuroimaging findings indicate that the migraine aura is due to cortical spreading depression (CSD), a wave of transient intense spike activity that progresses slowly along the cortex and is followed by a long-lasting neuronal suppression.[3-6] It is unknown what makes the migraine brain more susceptible to CSD.

Why and how migraine attacks begin is unknown, but CSD may play a role. CSD has been shown to activate the trigeminovascular system in animal models.[7] Alternatively, activation of certain brainstem nuclei may play an initiatory role as well.[8,9]

Familial Hemiplegic Migraine (FHM) is an autosomal dominant subtype of migraine with aura. Apart from the characteristic hemiparesis, typical attacks of FHM are identical to those of the common forms of migraine.[10] In addition, more than two thirds of patients with FHM also have attacks of "normal typical migraine". This makes FHM a promising

model also to study the pathogenesis of the common forms of migraine. In over half of the families, FHM is caused by missense mutations in the *CACNA1A* gene on chromosome 19p13, FHM-1 (OMIM 141500).[11,12] The *CACNA1A* gene encodes the pore forming α1 subunit of voltage-gated neuronal $Ca_v2.1$ (P/Q-type) Ca^{2+} channels.[12] Fifteen different missense mutations in the *CACNA1A* gene have been associated with FHM. Some mutations cause pure FHM whereas other mutations may cause FHM plus additional neurological symptoms such as ataxia or coma.[13,14] All mutations result in substitutions of conserved amino acids in important functional regions including the pore lining and the voltage sensors of the channel protein. $Ca_v2.1$ channels are located throughout the mammalian nervous system[15] at presynaptic terminals where they play a prominent role in controlling neurotransmitter release[16,17] and at somatodendritic membranes, where they also exert post-synaptic effects, such as on neuronal excitability.[18] $Ca_v2.1$ channels are expressed in all brain structures that have been implicated in the pathogenesis of migraine including the cerebral cortex, the trigeminal ganglia, and brainstem nuclei involved in the central control of nociception (for review see[2]).

The functional consequences of FHM-1 mutations have been investigated by expressing recombinant $Ca_v2.1$ channel subunits in heterologous systems and in cerebellar granule cells from $Ca_v2.1$-α_1 knockout mice.[19-21] The results, however, differed between the various expression systems and the functional effects found in neurons were apparently contradicting: *gain-of-function* in single human $Ca_v2.1$ channels (with increased Ca^{2+} influx in a broad voltage range as a consequence of their activation at lower voltages) and *loss-of-function* at the whole-cell level due to reduced density of functional $Ca_v2.1$ channels in the membrane.[21] It therefore is important to study mutant $Ca_v2.1$ channels in their native neuronal environment at their endogenous level of expression when they are expressed in knockin (KI) animals. Such models will also allow evaluating the consequences of FHM-1 mutations on mechanisms involved in migraine such as neurotransmission and cortical spreading depression.

Here, we generated a KI mouse model with the human R192Q pure FHM-1 mutation by using a gene-targeting approach. This FHM phenotype is closest to that of the common forms of migraine. Functional analysis revealed a pure *gain-of-function* effect on Ca^{2+} channel current, neurotransmission, and cortical spreading depression. These results may explain the underlying mechanism for the increased susceptibility of the migraine brain for CSD and aura and reinforce the hypothesis that migraine is associated with neuronal hyperexcitability at the cortical and, possibly, brainstem level.

Experimental procedures

Generation of R192Q KI transgenic mice

First, R192Q KI +NEO mice (see Figure 1A for details) were generated, using homologous recombination in ES cells to modify the *Cacna1a* gene such that the exon 4 contained the human FHM1 R192Q mutation. Mouse genomic DNA clones were derived from a pPAC4 library (129/SvevTACfBr strain). In the targeting vector the original CGG triplet codon 192 was changed into CAG by mutagenesis, creating the R192Q mutation. Downstream of exon 4, a PGK-driven *neo* cassette flanked by LoxP sites was present. Embryonic stem cells (E14) were electroporated and clones were selected for homologous recombination by Southern blot analysis using external probes. The presence of the R192Q mutation was tested by PCR using primers 5'-TGTCGGGACGGAGTTTGAC-3'and 5'-AGACTCACGCACTTGGGATT-3' and subsequent digestion with restriction enzyme the *AlwN*I as well as sequencing analysis of exon 4. Targeted ES cells were injected into blastocysts to create chimaeric animals. F1 agouti progeny was genotyped for transmission of the mutant allele, generating transgenic line R192Q KI +NEO. Heterozygous R192Q KI +NEO mice were bred with mice of the EIIA-*Cre* strain[22] to remove the *neo* cassette. Germline transmission was obtained and transgenic line R192Q KI was established (see Figure 1A). Mice were further bred with C57Bl/6J for five generations. Homozygous R192Q KI and wt littermates were used for further analysis (~97% C57Bl6J background), unless stated otherwise. All animal experiments were performed in accordance with the guidelines of the respective Universities and national legislation.

RNA analysis

Total RNA was isolated from forebrain or cerebellum using RNA Instapure (Eurogentec, Seraing, Belgium). For RT-PCR, first-strand cDNA was synthesized using random primers and subsequent PCR was performed using *Cacna1a* and *Cyclophilin* specific primers (primer sequences are available from the authors upon request). PCR products of *Cacna1a* and *Cyclophilin* were used to probe the Northern blot using standard conditions.

Western blot analysis

To prevent proteolysis during the procedure, all steps were carried out on ice, and all buffers contained protease inhibitor cocktail (Cat No 1 836 170, Roche, Mannheim, Germany) and phenylmethanesulfonyl fluoride (1 mM). Brains of the various genotypes were processed simultaneously. For the extraction of membrane proteins, whole cerebella

were homogenized with a glass-Teflon homogenizer in 500 µl working solution (50 mM HEPES pH 7.4/1 mM EGTA). After a short centrifugation (5 min 20,000 rpm, Beckmann TLA 120.1), the supernatant was centrifuged for 1,5 h at 58,000 rpm (Beckmann TLA 120.1). The membrane fractions were resuspended in 80 µl 2x Sample buffer (100 mM Tris-Glycine pH 6.8, 0.56 M β-mercaptoethanol, 2% SDS, 15% glycerol, and 0.1% BFB) and incubated for 10 min at 75 ºC. Protein fractions were loaded onto 4-15% gradient SDS-PAGE. After separation, proteins were transferred onto a nitrocellulose membrane (0.2 µm). Blots were blocked with PBS/5% low fat milk/0.05% Tween-20 and subsequently incubated o/n with primary $Ca_v2.1$-α_1 antibody (AB5152, Chemicon, Temecula, CA, USA) (1:200 diluted in incubation buffer (PBS/0.05% Tween-20)) together with primary actin antibody (A2066, St Louis, MO, USA) (1:1000 diluted in incubation buffer) at room temperature. Secondary peroxidase-labelled goat anti-rabbit antibody (Cat. nr. 111-035-003, Jackson ImmunoResearch Laboratories, West Grove, PA, USA) (1:1000 diluted in incubation buffer) incubation was performed for 1 hour at room temperature. Western blotting was done according to the enhanced chemiluminescence ECL protocols (Amersham). Semi-quantification was based on equal β-actin signal intensity.

Histology

Brains from adult mice (~3 months-old) were fixed in 4% PFA for 2 hours. Paraffin sections (5 µm) were prepared and stained with Klüver-Barrera staining using standard protocols.

Immunohistochemistry

Brains of adult mice (~3 months-old) were obtained after perfusion with PBS followed by 4% PFA fixation. Post-fixation was done for 1 to 2 hours in 4% PFA followed by o/n incubation in 10% sucrose/0.1 M phosphate buffer at 4 ºC. Subsequently, membranes were removed, tissue was embedded in 10% sucrose/11% gelatine, and gelatin was fixed with 30% sucrose/10% formaline for 2.5 hours at room temperature, followed by o/n incubation in 30% sucrose/0.1 M phosphate buffer at 4 ºC. After freezing down, coronal sections of 40µm were processed free-floating during whole procedure. For immunohistochemistry, antigen retrieval was performed for 30 min at 80 ºC in 10 mM citrate buffer (pH 5.5). Sections were incubated in 10% heat-inactivated FCS/0.5%TX100/TBS for 2 hours and then incubated with primary $Ca_v2.1$-α_1 antibody (#ACC-001, Alomone Labs, Jerusalem, Israel) (1:200 diluted in 2% heat-inactivated FCS/ 0.4%TX100/TBS at 4 ºC. Secondary biotin-labeled goat anti-rabbit antibody (Vector Laboratories, Burlingame, CA) (1:200 diluted in the same buffer) incubation was performed for 2 hours at room temperature. Finally, for detection, sections were incubated with the avidin-biotin kit (Vector

Laboratories, Burlingame, CA) for 2 hours at room temperature, washed, and developed in 0.1 mg/ml diaminobenzidine with 0.005% H_2O_2.

Electrophysiology of cerebellar granule cells

Cerebellar granule cells were grown in primary culture from 6-day-old mice as described (Fletcher et al., 2001). Experiments were performed on cells grown from 6 to 7 days *in vitro*. Whole-cell patch-clamp recordings were performed at room temperature as in Fletcher *et al*.[23] External recording solution: 5 mM $BaCl_2$, 148 mM tetraethylammonium (TEA)–Cl, 10 mM Hepes (pH 7.4 with TEA-OH) and 0.1 mg/ml cytochrome C. Internal solution: 100 mM Cs-methanesulfonate, 5 mM $MgCl_2$, 30 mM Hepes, 10 mM EGTA, 4mM ATP, 0.5 mM GTP and 1 mM c-AMP (pH 7.4 with CsOH). Currents were sampled at 5 kHz and low-pass filtered at 1 kHz. Compensation (typically 70%) for series resistance was generally used. Current-voltage (I-V) relationships were obtained only from cells with a voltage error of <5 mV and without signs of inadequate space clamping such as notch-like current discontinuities, slow components in the decay of capacitative currents (in response to hyperpolarizing pulses) or slow tails not fully inhibited by nimodipine. The average normalized I-V curves were multiplied by the average maximal current density obtained from all cells. I-V curves were fitted with Eq. 1: $I = G\,(V-E_{rev})\,(1+\exp((V_{1/2}-V)/k))^{-1}$ using a non-linear regression method based on the Levenberg-Marquardt algorithm.

The liquid junction potentials were such that a value of 12 mV should be subtracted from all voltages to obtain the correct values of membrane potential in whole-cell recordings.[23] Averages are given as mean ± SEM.

All drugs were stored as stock solutions at –20 °C: 250 μM ω-conotoxin-GVIA (ω-CgTx-GVIA, Bachem, Budendorf, Switzerland) and 250 μM ω-conotoxin-MVIIC (ω-CTx-MVIIC, Bachem, Budendorf, Swizerland) in distilled water, 10 mM nimodipine (gift from Dr. Hof, Sandoz, Basel, Switzerland) in 95% ethanol.

Ex vivo electrophysiological recordings at the neuromuscular junction

Mice (male and female; 20-30 g; ~3 months-old) were euthanized by carbon dioxide inhalation. Phrenic nerve-hemidiaphragms were dissected and mounted in standard Ringer's medium (116 mM NaCl, 4.5 mM KCl, 2 mM $CaCl_2$, 1 mM $MgSO_4$, 1 mM NaH_2PO_4, 23 mM $NaHCO_3$, 11 mM Glucose, pH 7.4) at room temperature. In some experiments lower $CaCl_2$ concentrations were used. Intracellular recordings of miniature endplate potentials (MEPPs, the spontaneous depolarizing events due to uniquantal ACh release) and endplate potentials (EPPs, the depolarization resulting from nerve action potential-evoked ACh release) were made at neuromuscular junctions (NMJs) at

28 °C using standard micro-electrode equipment, as described previously.[24] At least 30 MEPPs and EPPs were recorded at each NMJ, and at least 10 NMJs were sampled per experimental condition per mouse. Muscle action potentials, mediated by Na^+ channels, were blocked by 2.3 μM of the selective muscle Na^+ channel blocker μ-Conotoxin GIIIB (Scientific Marketing Associates, Barnet, Herts, U.K.). In order to record EPPs, the phrenic nerve was stimulated supramaximally at 0.3 Hz. The amplitudes of EPPs and MEPPs were normalized to –75 mV, assuming 0 mV as the reversal potential for ACh-induced current.[25] The normalized EPP amplitudes were corrected for non-linear summation according to McLachlan and Martin[26] with an f-value of 0.8. Quantal content, i.e. the number of ACh quanta released per nerve impulse, was calculated by dividing the normalized and corrected mean EPP amplitude by the normalized mean MEPP amplitude.

In order to assess the contribution of P-type currents on ACh release, EPPs and MEPPs were also measured in the presence of 200 nM of the P-type-selective Ca^{2+} channel blocker ω-Agatoxin-IVA (Scientific Marketing Associates, Barnet, Herts, U.K.) during a 45 min measuring period, following a 15 min pre-incubation with the toxin.

Statistical significance was assessed using paired or unpaired Student's t-tests, where appropriate, on the grand mean values with *n* as the number of mice tested, and with 10-15 NMJs tested per muscle. All experiments were performed blind to the genotypes.

Cortical Spreading Depression

Mice (male and female; 20-30 g) were anaesthetized with urethane (20% in saline; 6 ml/kg i.p.). Wildtype and homozygous KI mice were fed equally and no difference in body weight was observed between the two genotypes. The mice were not fasted prior to CSD recordings. For each recording session four littermates, two R192Q KI mutants and two wt were analyzed; the genotypes were disclosed at the end of the recording session. Animals that were mounted on a stereotaxic apparatus were continuously monitored for adequate level of anesthesia, temperature, stable heart rate and nociceptive reflexes during the 100-150 min duration of the experiments. To record CSD three holes were drilled in the skull over the left hemisphere at the following coordinates (mm from bregma): (1) electrical stimulation: posterior 5 mm, lateral 3.5; (2) micropipette 1: posterior 0.7 mm, lateral 1.4; (3) micropipette 2: anterior 1.5 mm, lateral 1.2 (Figure 5A). The steady (DC) potential was recorded with glass micropipettes mounted on a computerized micromanipulator (Marzhauser, D) 200 μm below the dural surface (tip resistance 1–2 MΩ). An Ag/AgCl electrode was placed subcutaneous above the nose. After electrode insertion, DC potential was recorded for 10 minutes prior to cortical stimulation. Afterwards, the first electrical stimulation was delivered (10 microAmp for

100 msec) by means of a silver bipolar electrode (500 μm tip diameter, 0.8 mm inter-tip distance) placed on the dura. A stimulus isolator/constant current unit (WPI, USA) was used to generate the stimulation current. The DC potential was then recorded for 5 minutes. If CSD was not elicited, 100 ms long pulses of increasing intensity (20, 30, 40, 50, 60, 80, 100, 150, 200, 300, 400, 500, 600, 800 microAmp) were applied at 5 minutes interval until a CSD was elicited. The charge (current intensity times stimulus duration) delivered with the first stimulation activating a CSD was then taken as CSD threshold. Cortical potentials were amplified and low pass filtered at 100 Hz (Cyberamp, Axon Instruments, CA, USA). Signals were continuously digitized and recorded using Labview data acquisition and analysis system. To estimate CSD propagation velocity, at the end of the experiment the distance between the recording electrodes was accurately measured using the motorized manipulator (0.1 μm step) and this value was divided by the time elapsing between the CSD onset at electrode 1 and 2. CSD duration was measured at half-peak amplitude.

Results

Generation of R192Q Knock-in Mice

We introduced the human R192Q (FHM-1) mutation at the corresponding position in the mouse ortholog *Cacna1a* gene, encoding the $Ca_v2.1$-α_1 subunit, by homologous recombination (Figure 1A). Chimaeric mice were born and transmitted the R192Q KI +NEO allele through the germ line. In addition to the R192Q mutation, the mice contained the *neo* cassette, flanked by loxP-sites. R192Q KI +NEO mice are fertile and show no overt phenotype. To delete the *neo* cassette, we crossed the mice with transgenic mice expressing Cre recombinase under the control of the adenovirus EIIA early promoter.[22] Expression of Cre protein in early embryos permitted reciprocal recombination at the loxP sites resulting in removal of the *neo* cassette leaving only one loxP site. By subsequent breeding of the heterozygous R192Q KI mice with C57Bl6J the *Cre* transgene was selected against. Finally, homozygous R192Q KI mice were generated by interbreeding of R192Q KI heterozygous mice. Heterozygous and the homozygous mice are viable and breed normally (data not shown). Unlike the existing natural $Ca_v2.1$ mutant mouse strains, which show a clear phenotype of epilepsy and/or ataxia[27], the homozygous R192Q KI mice do not exhibit an overt phenotype. Correct homologous recombination in the homozygous R192Q KI mice was confirmed by Southern-blot analysis (Figure 1B). Expression of mutant *Cacna1a* mRNA was shown by sequencing of RT-PCR products of cerebellar cDNA (Figure 1C) and Northern-blot analysis (Figure 1D). Semi-quantitative Western blot analysis, using actin as a standard, revealed equal amounts of proteins for

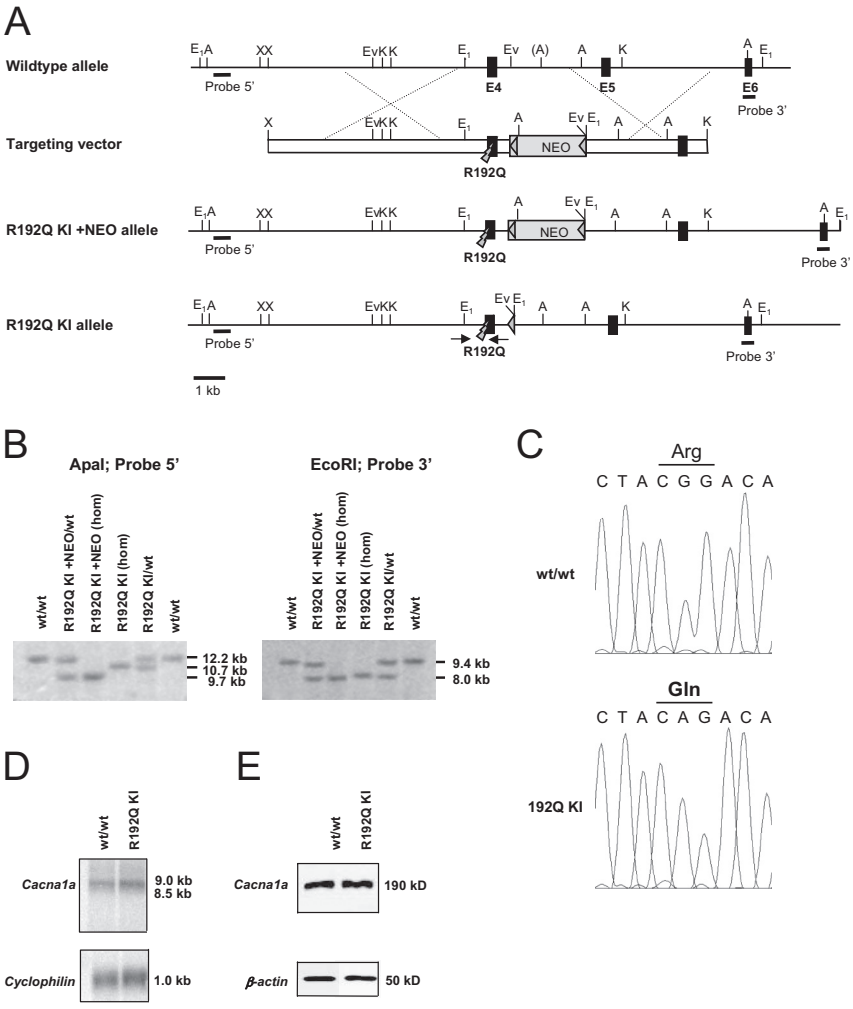

Figure 1. Generation of R192Q knockin (KI) mice. (**A**) Relevant part of genomic structure of the wt *Cacna1a* allele, targeting vector and predicted structure after homologous recombination (R192Q KI +NEO allele), and after Cre-mediated deletion of the Neo-cassette (depicted as gray box) (R192Q KI allele). LoxP sites are indicated by triangles. Black boxes indicate respective exons, with the R192Q mutation in exon 4 (E4). Black horizontal lines indicate probes for Southern and Northern. Primers used for genotyping and confirmation of the R192Q mutation are depicted schematically by a pair of arrows. Restriction sites: EI, EcoRI; EV, EcoRV; K, KpnI; A, ApaI; X, XbaI. (A) indicates an ApaI site that is polymorphic between the construct and wt allele. (**B**) Southern blot of R192Q KI +NEO and R192Q KI mutants. ApaI- and EcoRI-digested genomic DNA from three genotypes for R192Q KI +NEO and R192Q KI strains probed either the 5'- or 3'-probe. Hom: homozygote. (**C**) Sequencing analysis of RT-PCR products of cerebellar mRNA isolated from wt and homozygous R192Q KI mutant mice. (**D**) Northern blot of mRNA isolated from adult forebrain of wt and homozygous R192Q KI mice hybridized with either the *Cacna1a* or the *Cyclophilin* cDNA probe. (**E**) Semi-quantitative Western blot of cerebellar membrane protein extracts isolated from wt and homozygous R192Q KI mice probed with $Ca_v2.1$ and actin antibody. Equal levels of $Ca_v2.1$-α_1 protein are present in wt and homozygous R192Q KI mice.

the mutant and wildtype $Ca_v2.1$-α_1 protein (Figure 1E). No apparent cytoarchitectural abnormalities were observed by standard histochemical stainings in brains of homozygous R192Q KI mice (data not shown). Coronal sections of the cerebellum, with cell layers that can be distinguished with Klüver-Barrera staining (Figures 2A, 2E), were analyzed because of their high expression of $Ca_v2.1$-α_1 protein. Immunohistochemistry showed a normal cerebellar expression pattern for $Ca_v2.1$-α_1 protein in the homozygous R192Q KI and wildtype (wt) mice with a high expression in the molecular cell layer and in Purkinje cells (Figures 2B-2C, 2F-2G). Representative coronal sections show a relatively high expression of $Ca_v2.1$-α_1 protein in the hippocampal areas and a low overall staining in, for instance, the cortical regions (Figures 2D, 2H).

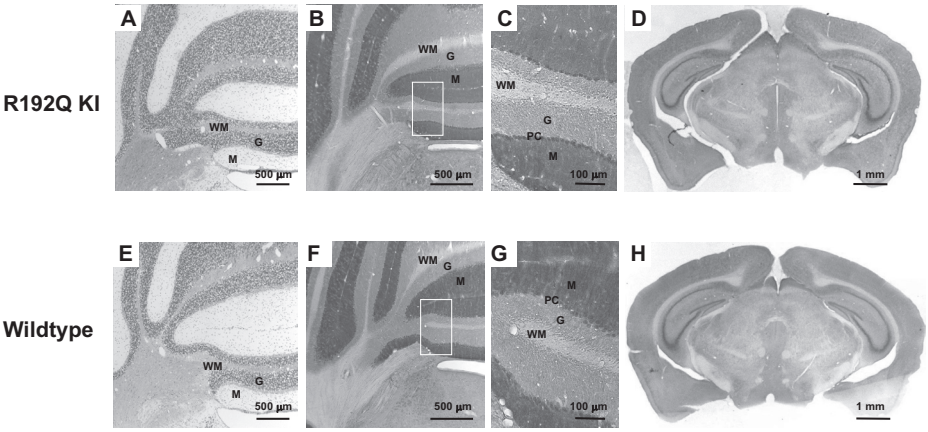

Figure 2. Histology and expression of $Ca_v2.1$ protein in homozygous R192Q KI mutants. (**A,E**) Coronal sections from cerebellum of homozygous R192Q KI and wildtype mice stained with Klüver-Barrera. (**B,F**) Immunostaining of $Ca_v2.1$-α_1 protein in homozygous R192Q KI and wildtype cerebellum (enlarged section in (**C,G**)). (**D,H**) Immunostaining of $Ca_v2.1$-α_1 protein of coronal section showing a relatively high expression in the hippocampus and low overall staining in the cortical regions of homozygous R192Q KI brain. No differences in expressing level and pattern of $Ca_v2.1$-α_1 protein, or apparent overall structural abnormalities were observed between both genotypes. Scale bars are depicted. WM: white matter; G: granule cell layer; M: molecular cell layer PC: Purkinje cell layer.

Gain-of-function Effects of the R192Q Mutation on Neuronal Ca^{2+} Current

We investigated the consequences of the R192Q mutation on $Ca_v2.1$ channel function by measuring the $Ca_v2.1$ current density as a function of voltage in cerebellar granule cells in primary culture from homozygous R192Q KI and wt mice (Figure 3). To isolate the component of whole-cell Ca^{2+} current that is due to $Ca_v2.1$ channels, ω-conotoxin MVIIC (MVIIC; 3 µM), a toxin that inhibits both N- and P/Q-type calcium channels, was applied after subsequent additions of saturating concentrations of nimodipine (L-type channel blocker; 5 µM) and the specific blocker of N-type channels, ω-CgTx-GVIA

(1μM) (Figure 3A).[21] This protocol enabled measurement of the L-, N- and R-type components of the Ca^{2+} current in addition to the P/Q-type component.

The $Ca_v2.1$ current density in R192Q KI neurons was larger than in wt neurons over a broad voltage range (Figure 3B). The relative increase in R192Q KI current density was larger at lower voltages close to the threshold of channel activation and progressively diminished with increasing voltages. The voltage dependence of the relative increase in R192Q KI current density is consistent with mutant $Ca_v2.1$ channels being activated at more negative voltages than wt channels. Fitting of the current-voltage relationship curves gave half-voltage of activation values ($V_{1/2}$) of –13.9 ± 0.9 mV for the wt and of –22.7 ± 0.5 mV for the mutant channels. The kinetics of activation of the $Ca_v2.1$ current in R192Q KI neurons was faster than in wt neurons (traces and inset of Figure 3B). The

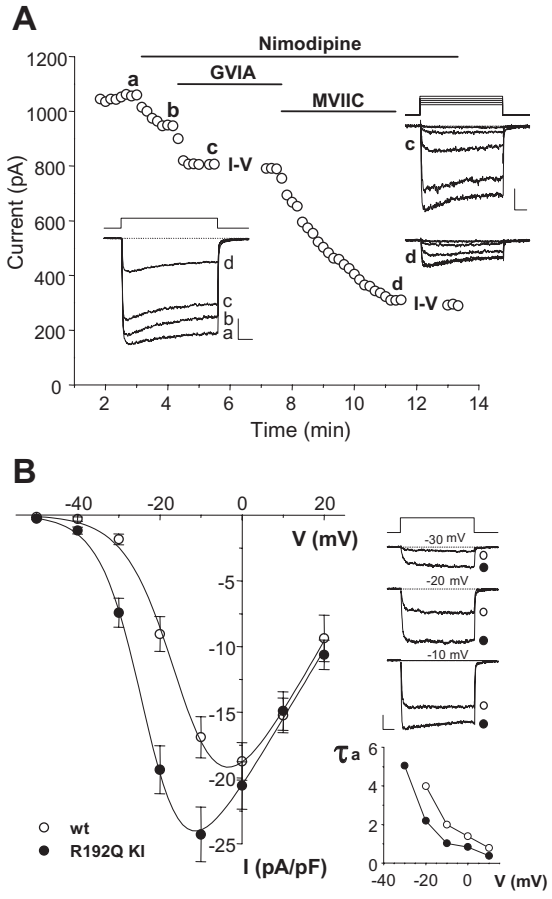

Figure 3. Increased $Ca_v2.1$ current density in cerebellar granule cells of homozygous R192Q KI mice. (**A**) Peak whole-cell Ba^{2+} current vs. time recorded from a R192Q KI cerebellar granule cell during depolarizations at –10 mV every 10 s from –80 mV, before and after application of the indicated drugs. Inset: representative traces taken at times a, b, c, d. On the right: representative traces at increasing voltage from –50 to –10 mV taken during current-voltage (I-V) relationships measured at times c and d. Bars: 20 ms, 200 pA. $Ca_v2.1$ currents were obtained as the difference between traces at times c and d. (**B**) $Ca_v2.1$ current density, I, as a function of voltage in wt and R192Q KI granule cells. Average normalized I-V curves (n = 9 for wt and n = 12 for KI) were multiplied by the average maximal current density (n = 27 for wt and n = 39 for KI). Solid lines are fits of equation 1 in Methods. Inset: Pooled wt and KI $Ca_v2.1$ current traces at –30, -20 and –10 mV (Bars: 20 ms, 5 pA/pF) and corresponding time constants of current activation (τ) as a function of voltage.

shifted voltage dependence of the time constant (τ) of activation (inset of Figure 3B) is consistent with the conclusion that mutant channels activate at lower voltages and open more readily than wt channels.

In contrast with the finding in cerebellar granule cells isolated from $Ca_v2.1$-α_1 knockout mice and transfected with mutant human $Ca_v2.1$-α_1 subunits[21], the R192Q mutation did not decrease the density of functional $Ca_v2.1$ channels in the granule cells of the R192Q KI mouse. Given that the R192Q mutant and wt channels have identical single channel current and similar maximal open probability[19], a similar density of functional channels can be inferred from the similar $Ca_v2.1$ current densities in R192Q KI and wt granule cells at voltages higher than 0 mV (Figure 3B), where open probabilities are maximal for both mutant and wt channels.[21]

The densities of the L-, N- and R-type components of the Ca^{2+} current were not significantly different in R192Q KI and wt granule cells: L-type: 11.3 ± 0.9 (n = 30) and 13.8 ± 1.5 (n = 20) pA/pF; N-type: 6 ± 0.6 (n = 30) and 5.2 ± 0.6 (n = 22) pA/pF; R-type 23.7 ± 1.8 (n = 39) and 23.4 ± 1.3 (n = 27) pA/pF. Therefore, granule cells of the homozygous R192Q KI mice do not show alterations of other Ca^{2+} channels as a mechanism for compensation of the *gain-of-function* of $Ca_v2.1$ channels.

Enhanced evoked and spontaneous Neurotransmitter release at Neuromuscular Junction of R192Q KI Mice

$Ca_V2.1$ channels play a prominent role in controlling neurotransmitter release in many synapses of the mammalian nervous system. Given the fourth-power dependence of neurotransmitter release on intracellular Ca^{2+} concentration, small changes in amplitude or time course of Ca^{2+} influx at the release sites are expected to be very effective in modulating transmitter output at those synapses where the Ca^{2+} sensors are not saturated during an action potential.[28] This predicts that at such synapses $Ca_V2.1$ channels that open more readily and at lower voltages because of the R192Q mutation lead to an increased action potential-evoked Ca^{2+} influx and a consequent increase in neurotransmitter release. To test this hypothesis, we studied neurotransmission at the neuromuscular junction (NMJ), a single synapse that shares with many central synapses the location of $Ca_V2.1$ channels at the release sites close to the presynaptic Ca^{2+} sensors[16,17,29] and a similar cooperative action of Ca^{2+} ions in controlling transmitter release.[28,30,31]

Endplate potentials (EPPs), representing the postsynaptic depolarizations produced by the acetylcholine (ACh) release evoked by a single action potential, were measured at both physiological concentrations of Ca^{2+} ions, probably leading to saturation of the NMJ Ca^{2+} sensors[29] and at lower concentrations not saturating the Ca^{2+} sensors. The amount of ACh released from nerve terminals at low-rate stimulation (0.3 Hz) did not

differ between genotypes when measured at 2 mM Ca^{2+} (Figure 4A). The quantal content was 42.5 ± 1.7 and 42.6 ± 2.3 at wt (n = 13**,** number of mice tested) and homozygous R192Q mutant (n = 12) NMJs, respectively (p = 0.97). Also the kinetics of EPPs did not differ between genotypes, and the P/Q-type Ca^{2+} channel blocker ω-Agatoxin-IVA (200 nM) reduced quantal contents equally at both wt and R192Q mutant NMJs by ~90% (Figures 4A-4B). No differences in quantal content were found at 1 mM Ca^{2+} (Figure 4A). However, when the Ca^{2+} concentration was reduced to 0.2 mM the quantal content was ~240% higher at homozygous R192Q KI NMJs (5.0 ± 0.9 and 17.1 ± 4.1 at wt (n = 7) and R192Q mutant (n = 7) NMJs, respectively ($p < 0.05$)) (Figure 4A).

At the wt NMJ, $Ca_V2.1$ channels are also involved in controlling a fraction of spontaneous quantal ACh release, since the frequency of the miniature endplate potential (MEPP, the spontaneous postsynaptic depolarizing event resulting from uniquantal ACh release) is sensitive to ω-Agatoxin-IVA (Figure 4C).[24] At NMJs of homozygous R192Q KI mice, MEPP frequency was found increased by 81% compared to wt controls (2.13 ± 0.15 and 1.18 ± 0.07/s, respectively, $p < 0.001$, n = 20, Figures 4C-4D). Addition of 200 nM ω-Agatoxin-IVA reduced the MEPP frequency at wt and R192Q KI NMJs by 44% and 68% (n = 10, $p < 0.001$), respectively, to almost equal values (0.62 ± 0.04 and 0.66 ± 0.04/s at wt and R192Q KI NMJs, respectively, p = 0.53, Figure 4C). Interestingly, in a second series of experiments, the MEPP frequency of heterozygous mice had an intermediate value (1.66 ± 0.16/s) between those of wt and homozygous R192Q KI mice (1.00 ± 0.13/s and 2.45 ± 0.30/s, respectively, n = 4-6 mice, $p < 0.05$ between all three groups).

The difference in MEPP frequency between genotypes became more pronounced upon slight depolarization of nerve terminals by 10 mM K^+, increasing the MEPP frequency in homozygous R192Q KI NMJs to 425% of wt controls (24.48 ± 2.26/s (n = 17) and 5.76 ± 0.53/s (n = 19) at R192Q KI and wt NMJs, respectively) (Figures 4C-4D). ω-Agatoxin-IVA reduced MEPP frequency by 81% and 92% at wt and R192Q KI NMJs, respectively to almost equal values (n = 10, Figures 4C-4D) Thus, the analysis of both evoked and spontaneous ACh release indicates that the R192Q FHM-1 mutation leads to enhanced neurotransmission in synapses under conditions in which the synaptic Ca^{2+} sensors are not saturated. Furthermore, the intermediate synaptic phenotype of heterozygous NMJs observed with MEPP frequency, indicates an allele-dose effect, which is in accordance with dominance of the mutation in FHM patients.

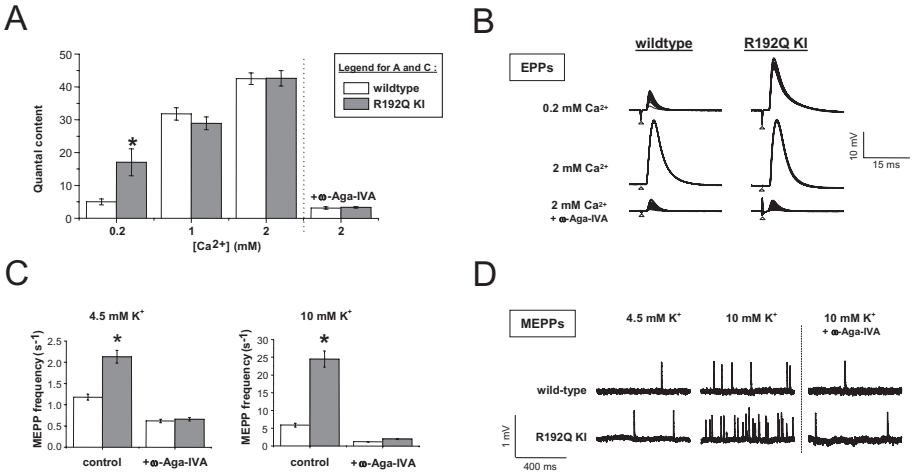

Figure 4. Increased neurotransmitter release at homozygous R192Q KI neuromuscular synapses. (**A**) Quantal content (upon 0.3 Hz nerve stimulation) at wt and homozygous R192Q KI neuromuscular junctions (NMJs), measured with 0.2, 1, or 2 mM Ca^{2+} in the Ringer's medium. Values obtained at 1 and 2 mM Ca^{2+} did not differ between genotypes. At 0.2 mM Ca^{2+}, however, the quantal content was found to be much higher at R192Q KI NMJs than at wt controls (~240% increase, n = 7 mice, p <0.05). ω-Agatoxin-IVA (200 nM) caused a reduction of ~90% on quantal content at 2 mM Ca^{2+} in both R192Q KI and wt NMJs. (**B**) Typical examples of endplate potentials (EPPs) recorded upon 0.3 Hz nerve stimulation in the different Ca^{2+} concentrations and in the presence of ω-Agatoxin-IVA (20 consecutive EPPs superimposed; the point of stimulation is indicated by arrow heads. (**C**) Spontaneous quantal ACh release was found increased by 81% at homozygous R192Q KI NMJs (n = 20 mice, p <0.001) compared to wt NMJs, when measured as miniature endplate potential (MEPP) frequency in normal Ringer's medium containing 4.5 mM K^+. This difference became more pronounced upon slight depolarization of nerve terminals by 10 mM K^+, increasing MEPP frequency in R192Q KI NMJs to 425% of wt controls (n = 17 mice, p <0.001). ω-Agatoxin-IVA greatly reduced MEPP frequency and eliminated the observed differences between the genotypes. (**D**) Typical examples of MEPPs recorded at wt and R192Q KI NMJs. * indicates a statistically significant difference.

Lowered threshold and increased velocity for Cortical Spreading Depression (CSD) in R192Q KI Mice

As mentioned earlier, CSD is the likely mechanism of migraine aura[3-6] and can activate the trigeminovascular system in animal models.[7] Therefore, we analyzed the *in vivo* threshold for initiation, rate of propagation and duration of CSD in anaesthetized mice by electrical stimulation of the visual cortex through a bipolar electrode (Figure 5A). The steady (DC)-potential was recorded at two cortical sites located in the primary somatosensory and motor cortex. Stimulation current pulses of increasing intensity were applied at 5 minutes interval until a CSD was observed. The charge (current intensity times stimulus duration) delivered with the first stimulation activating a CSD was then taken as CSD threshold.[32] Homozygous R192Q KI mutants were more prone to CSD induction than their wt littermates, as significantly less charge needed to be delivered

to the cortex to elicit CSD in R192Q KI mutants than in wt (7.9 ± 2.0 μC, n =14 vs. 28 ± 7.6 μC, n =13, respectively; Mann-Whitney test, p <0.01). A cumulative distribution of CSD threshold for the two genotypes is shown in Figure 5B. To investigate whether the R192Q mutation affected aspects of CSD other than initiation, we also measured the velocity of CSD propagation between the two recording electrodes and CSD duration. The R192Q mutation resulted in a ~150% increase of CSD velocity from 3.2 ± 0.13 mm/min in wt to 4.6 ± 0.17 mm/min in R192Q KI mutant animals (t-test, p <0.001) (Figure 5C). CSD duration was longer in R192Q KI mutants (86 ± 11 s) than in wt animals (50 ± 11 sec) although this difference did not reach statistical significance (Mann-Whitney test, p = 0.1).

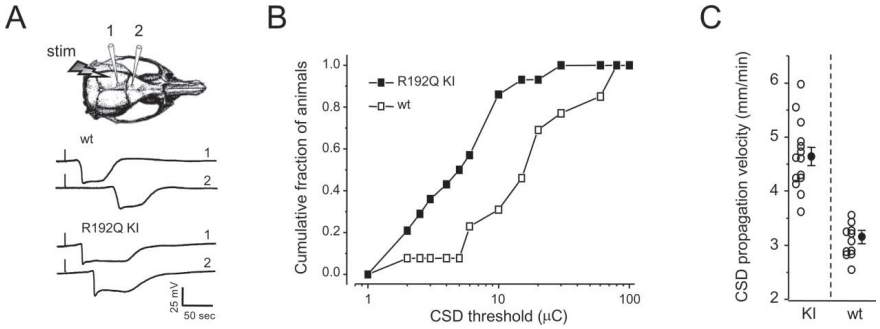

Figure 5. R192Q mutation facilitates the induction and the propagation of CSD. (**A**) Diagram indicating location of the stimulating and recording electrodes. Examples of the CSD recordings at sites 1 and 2 are shown. Note the high velocity of propagation and the long duration of CSD in the homozygous R192Q KI mutant with respect to wt. (**B**) Cumulative distribution of CSD threshold in homozygous R192Q KI mutant (n = 14) and wt (n = 13) mice. The plot displays the fraction of animals showing a CSD after electrical stimulation of intensity (expressed as charge obtained from current intensity times stimulus duration) minor or equal the corresponding value on the abscissa. The KI distribution is shifted to the left indicating that CSD was more easily inducible in KI than in wt (Kolmogorov-Smirnov test, p <0.01). (**C**) CSD propagation velocity (mm min^{-1}) is higher in homozygous R192Q KI than in wt mice (t-test, p >0.001). For each group, open circles represent values of single animals (n = 13, wt; n = 14, R192Q KI) and the filled circle represents the mean ± SEM.

Discussion

Here, we generated the first knock-in transgenic mice with the pathogenic FHM-1 mutation R192Q in the *Cacna1a* gene and evaluated the functional consequences for neuronal Ca^{2+} current, neurotransmission, and CSD. Our results allow several important conclusions.

First, the neuronal phenotype of the R192Q FHM-1 mutation (and most likely also others) is *gain-of-function* in terms of Ca^{2+} influx through both single $Ca_v2.1$ channels and the whole soma as a consequence of mutant channels that open more readily and at lower voltages than wt channels. This finding considerably simplifies the picture with respect to previous findings in transfected neurons. There, a *gain-of-function* was found at the single channel level, but *loss-of-function* at the whole-cell level as a consequence of a decreased number of functional channels.[21] In light of the unchanged density of *functional* channels when mutant $Ca_v2.1$ channels are expressed at their endogenous level in R192Q KI neurons, the alterations in *functional* channel density previously found in transfected neurons[21] and HEK293 cells[19] might have been an artefact due to overexpression. In any case, our data suggest that transfected cells (either HEK293 or neurons) are unreliable to study the consequences of ion channel mutations on the whole-cell current density. However, they can be reliably used to study the effect of mutations on the single channel function, given the similar alterations in channel gating produced by the R192Q mutation in transfected cells and KI neurons.[19,21]

Second, the *gain-of-function* phenotype of $Ca_v2.1$ channels was accompanied by

i. increased neurotransmission at the NMJ, in conditions where saturation of the synaptic Ca^{2+} sensors was not reached and the release probability was low (evoked release at low Ca^{2+} and spontaneous release), and

ii. increased susceptibility to CSD in the intact animal, as indicated by the lowered threshold for induction and the increased velocity of propagation.

Similar to the ACh release at the NMJ, release of the neuroexcitatory amino acid glutamate from cortical neurons depends predominantly on $Ca_v2.1$ (P/Q-type) channels.[33] On the other hand, $Ca_v2.1$ channels seem to play only a secondary role in controlling the cortical release of the inhibitory neurotransmitter GABA.[34] Many brain cortical excitatory synapses are characterized by a low probability of release in response to a single action potential.[28,35,36] Our data predict an increased action potential-evoked Ca^{2+} influx at the

active zones and an increased glutamate release at these synapses.

In line with this prediction is the strong decrease in intracortical glutamate concentration (with almost no change in GABA) measured by *in vivo* microdialysis during high K^+ exposure in the neocortex of the natural $Ca_v2.1$ mutant *leaner* mouse.[32] These mice have an electrophysiological phenotype opposite to that of the R192Q KI mutants. They carry a *loss-of-function* truncation mutation that shifts the channel activation curve towards less negative voltages and reduces the Ca^{2+} current density in neurons.[37,38] In addition, *leaner* mice display a striking elevation in the threshold for initiating CSD and a slower velocity and frequent failure of propagation of CSD.[32] These data are consistent with reduced cortical network excitability in *leaner* resulting from reduced release of glutamate (with relatively unchanged GABA release). In analogy, the lowered threshold for CSD in the homozygous R192Q KI mice might be due to increased cortical network excitability resulting from increased glutamate release. Since NMDA receptor antagonists may block the initiation and propagation of CSD, glutamate is likely to be involved in both aspects of CSD.[39] Opposite changes in glutamate release in *leaner* and KI mice might then explain the opposite changes in velocity of propagation of CSD observed in these mutants. However, since $Ca_v2.1$ channels are located also in somatodendritic membranes throughout the brain, postsynaptic mechanisms might also contribute to the changes in the CSD threshold and rate of propagation in KI mice. In summary, our data, together with those of Ayata et al.[32], support an important role of $Ca_v2.1$ channels in the initiation and spread of CSD, and point to cortical hyperexcitability as the basis for CSD susceptibility.

Functional brain imaging and magnetoencephalography have provided evidence that migraine aura arises from CSD, and transcranial magnetic stimulation, recordings of cortical potentials and psychophysics suggests an altered cortical excitability in migraineurs (for review see Pietrobon and Striessnig, 2003).[2] However, there is debate as to whether the cortex of migraineurs is hypo- or hyperexcitable, and what the underlying molecular and cellular mechanisms are for the altered cortical excitability and increased susceptibility for CSD. The data from our FHM-1 mouse model suggest cortical hyperexcitability due to excessive release of excitatory amino acids secondary to increased Ca^{2+} influx as the underlying mechanism in FHM.

In line with the suggested cortical hyperexcitability is also the recent observation that mutations in the *ATP1A2* gene resulting in a loss of Na^+,K^+-ATPase function are associated with chromosome 1 linked FHM-2.[40,41] Loss of Na^+,K^+-ATPase pump function may depolarize neurons. Impaired clearance of K^+ by astrocytes, where expression of the α_2-subunit of Na^+,K^+-ATPase is particularly high[42] and consequent increase of extracellular K^+ may facilitate cortical spreading depression (CSD).

It is generally recognized that the development of migraine headache depends on the activation of the trigeminovascular system including trigeminal afferents innervating the meninges (for review see Pietrobon and Striessnig, 2003).[2] If CSD can indeed activate these afferents, as suggested by animal experiments[7], CSD could be the trigger for migraine attacks and FHM-1 KI mice may thus provide a useful animal model for migraine. Our data predict that drugs that are capable of shifting the activation range of $Ca_v2.1$ channels to more depolarized voltages would make the cortex more resistant to CSD, and may thus be able to prevent migraine attacks.

Although the consequences of FHM-1 mutations on trigeminal nociception remain unexplored, one can predict that the *gain-of-function* synaptic FHM-1 phenotype may lead to hyperexcitability of nociceptive trigeminovascular pathways due to enhanced release of vasoactive neuropeptides from perivascular nerve endings and, possibly, facilitation of sensitization of second order central trigeminal neurons. In fact, within the trigeminovascular system, P/Q-type channels, together with N-type, control CGRP release from capsaicin-sensitive trigeminovascular afferents[43] and P/Q-type channels located in the brainstem periaquaductal grey (PAG) are involved in the descending central control of trigeminal pain perception.[44] This brainstem area is of particular interest because of the apparent overlap with the site of increased metabolic activity in PET scans during migraine attacks.[9] Dysfunction of brainstem nuclei might contribute to central hyperexcitability of trigeminal pathways and consequently increased pain transmission.[1]

In conclusion, we generated the first knockin migraine mouse model and showed a pure *gain-of-function* effect on Ca^{2+} current, neurotransmission, and CSD. These findings support the idea of migraine as a disorder of neuronal hyperexcitability at the cortical and brainstem level. The R192Q KI mouse may provide a promising model for testing novel therapeutic strategies for migraine aimed at decreasing neuronal hyperexcitability and/or preventing CSD.

Acknowledgements

We thank I. Hegeman and Dr. S. van Duinen for assistance in histochemistry; E. Putignano for technical assistance, Dr. S. Verbeek for ES cell injections, and Dr. C.L. Thompson (University of Durham, UK) for helpful discussions and advice on Western blot analysis. This work was supported by grants of the Netherlands Organization for Scientific Research (NWO), the European Community, & and the Migraine Trust (to R.F. and/or M.F.); Telethon Italy, Italian Ministry of Education University Research (PRIN, FIRB, and ST/CNR-MIUR) (to D.P.); the Prinses Beatrix Fonds, the Hersenstichting Nederland, and KNAW van Leersumfonds (to J.P.).

References

1. Goadsby,P.J., Lipton,R.B. & Ferrari,M.D. Migraine--current understanding and treatment. *N. Engl. J Med* **346**, 257-270 (2002).
2. Pietrobon,D. & Striessnig,J. Neurobiology of migraine. *Nat. Rev. Neurosci.* **4**, 386-398 (2003).
3. Bowyer,S.M., Aurora,K.S., Moran,J.E., Tepley,N. & Welch,K.M. Magnetoencephalographic fields from patients with spontaneous and induced migraine aura. *Ann. Neurol.* **50**, 582-587 (2001).
4. Cutrer,F.M. *et al.* Perfusion-weighted imaging defects during spontaneous migrainous aura. *Ann. Neurol.* **43**, 25-31 (1998).
5. Hadjikhani,N. *et al.* Mechanisms of migraine aura revealed by functional MRI in human visual cortex. *Proc. Natl. Acad. Sci. U. S. A* **98**, 4687-4692 (2001).
6. Lauritzen,M. Pathophysiology of the migraine aura. The spreading depression theory. *Brain* **117 (Pt 1)**, 199-210 (1994).
7. Bolay,H. *et al.* Intrinsic brain activity triggers trigeminal meningeal afferents in a migraine model. *Nat. Med.* **8**, 136-142 (2002).
8. Goadsby,P.J. Migraine, aura, and cortical spreading depression: why are we still talking about it? *Ann. Neurol.* **49**, 4-6 (2001).
9. Weiller,C. *et al.* Brain stem activation in spontaneous human migraine attacks. *Nat. Med.* **1**, 658-660 (1995).
10. Thomsen,L.L. *et al.* A population-based study of familial hemiplegic migraine suggests revised diagnostic criteria. *Brain* **125**, 1379-1391 (2002).
11. Joutel,A. *et al.* A gene for familial hemiplegic migraine maps to chromosome 19. *Nat. Genet.* **5**, 40-45 (1993).
12. Ophoff,R.A. *et al.* Familial hemiplegic migraine and episodic ataxia type-2 are caused by mutations in the Ca2+ channel gene CACNL1A4. *Cell* **87**, 543-552 (1996).
13. Ducros,A. *et al.* The clinical spectrum of familial hemiplegic migraine associated with mutations in a neuronal calcium channel. *N. Engl. J. Med.* **345**, 17-24 (2001).
14. Kors,E.E., van den Maagdenberg,A.M., Plomp,J.J., Frants,R.R. & Ferrari,M.D. Calcium channel mutations and migraine. *Curr. Opin. Neurol.* **15**, 311-316 (2002).
15. Westenbroek,R.E. *et al.* Immunochemical identification and subcellular distribution of the alpha 1A subunits of brain calcium channels. *J. Neurosci.* **15**, 6403-6418 (1995).
16. Mintz,I.M., Sabatini,B.L. & Regehr,W.G. Calcium control of transmitter release at a cerebellar synapse. *Neuron* **15**, 675-688 (1995).
17. Wu,L.G., Westenbroek,R.E., Borst,J.G., Catterall,W.A. & Sakmann,B. Calcium channel types with distinct presynaptic localization couple differentially to transmitter release in single calyx-type synapses. *J Neurosci.* **19**, 726-736 (1999).
18. Pineda,J.C., Waters,R.S. & Foehring,R.C. Specificity in the interaction of HVA Ca2+ channel types with Ca2+-dependent AHPs and firing behavior in neocortical pyramidal neurons. *J Neurophysiol.* **79**, 2522-2534 (1998).
19. Hans,M. *et al.* Functional consequences of mutations in the human alpha1A calcium channel subunit linked to familial hemiplegic migraine. *J. Neurosci.* **19**, 1610-1619 (1999).
20. Kraus,R.L., Sinnegger,M.J., Glossmann,H., Hering,S. & Striessnig,J. Familial hemiplegic migraine mutations change alpha1A Ca2+ channel kinetics. *J Biol. Chem.* **273**, 5586-5590 (1998).
21. Tottene,A. *et al.* Familial hemiplegic migraine mutations increase Ca(2+) influx through single human CaV2.1 channels and decrease maximal CaV2.1 current density in neurons. *Proc. Natl. Acad. Sci. U. S. A* **99**, 13284-13289 (2002).
22. Lakso,M. *et al.* Efficient in vivo manipulation of mouse genomic sequences at the zygote stage. *Proc. Natl. Acad. Sci. U. S. A* **93**, 5860-5865 (1996).
23. Fletcher,C.F. *et al.* Dystonia and cerebellar atrophy in Cacna1a null mice lacking P/Q calcium channel activity. *FASEB J.* **15**, 1288-1290 (2001).
24. Plomp,J.J. *et al.* Abnormal transmitter release at neuromuscular junctions of mice carrying the tottering alpha(1A) Ca(2+) channel mutation. *Brain* **123 Pt 3**, 463-471 (2000).

25. Magleby,K.L. & Stevens,C.F. A quantitative description of end-plate currents. *J. Physiol* **223**, 173-197 (1972).
26. McLachlan,E.M. & Martin,A.R. Non-linear summation of end-plate potentials in the frog and mouse. *J. Physiol* **311**, 307-324 (1981).
27. Fletcher,C.F. & Frankel,W.N. Ataxic mouse mutants and molecular mechanisms of absence epilepsy. *Hum. Mol. Genet.* **8**, 1907-1912 (1999).
28. Schneggenburger,R. & Neher,E. Intracellular calcium dependence of transmitter release rates at a fast central synapse. *Nature* **406**, 889-893 (2000).
29. Urbano,F.J. *et al.* Altered properties of quantal neurotransmitter release at endplates of mice lacking P/Q-type Ca2+ channels. *Proc. Natl. Acad. Sci. U. S. A* **100**, 3491-3496 (2003).
30. Dodge Jr,F.A. & Rahamimoff,R. Co-operative action a calcium ions in transmitter release at the neuromuscular junction. *J. Physiol.* ***193***, 419-432 (1967).
31. Wu,L.G. & Saggau,P. Presynaptic inhibition of elicited neurotransmitter release. *Trends Neurosci.* **20**, 204-212 (1997).
32. Ayata,C., Shimizu-Sasamata,M., Lo,E.H., Noebels,J.L. & Moskowitz,M.A. Impaired neurotransmitter release and elevated threshold for cortical spreading depression in mice with mutations in the alpha1A subunit of P/Q type calcium channels. *Neuroscience* **95**, 639-645 (2000).
33. Turner,T.J., Adams,M.E. & Dunlap,K. Calcium channels coupled to glutamate release identified by omega-Aga-IVA. *Science* **258**, 310-313 (1992).
34. Timmermann,D.B., Westenbroek,R.E., Schousboe,A. & Catterall,W.A. Distribution of high-voltage-activated calcium channels in cultured gamma-aminobutyric acidergic neurons from mouse cerebral cortex. *J Neurosci. Res.* **67**, 48-61 (2002).
35. Hessler,N.A., Shirke,A.M. & Malinow,R. The probability of transmitter release at a mammalian central synapse. *Nature* **366**, 569-572 (1993).
36. Reyes,A. *et al.* Target-cell-specific facilitation and depression in neocortical circuits. *Nat. Neurosci.* **1**, 279-285 (1998).
37. Dove,L.S., Abbott,L.C. & Griffith,W.H. Whole-cell and single-channel analysis of P-type calcium currents in cerebellar Purkinje cells of leaner mutant mice. *J. Neurosci.* **18**, 7687-7699 (1998).
38. Fletcher,C.F. *et al.* Absence epilepsy in tottering mutant mice is associated with calcium channel defects. *Cell* **87**, 607-617 (1996).
39. Somjen,G.G. Mechanisms of spreading depression and hypoxic spreading depression-like depolarization. *Physiol Rev.* **81**, 1065-1096 (2001).
40. De Fusco,M. *et al.* Haploinsufficiency of ATP1A2 encoding the Na+/K+ pump alpha2 subunit associated with familial hemiplegic migraine type 2. *Nat. Genet.* **33**, 192-196 (2003).
41. Vanmolkot,K.R. *et al.* Novel mutations in the Na+, K+-ATPase pump gene ATP1A2 associated with familial hemiplegic migraine and benign familial infantile convulsions. *Ann. Neurol.* **54**, 360-366 (2003).
42. Juhaszova,M. & Blaustein,M.P. Na+ pump low and high ouabain affinity alpha subunit isoforms are differently distributed in cells. *Proc Natl. Acad. Sci. U. S. A* **94**, 1800-1805 (1997).
43. Hong,K.W., Kim,C.D., Rhim,B.Y. & Lee,W.S. Effect of omega-conotoxin GVIA and omega-agatoxin IVA on the capsaicin-sensitive calcitonin gene-related peptide release and autoregulatory vasodilation in rat pial arteries. *J Cereb. Blood Flow Metab* **19**, 53-60 (1999).
44. Knight,Y.E., Bartsch,T., Kaube,H. & Goadsby,P.J. P/Q-type calcium-channel blockade in the periaqueductal gray facilitates trigeminal nociception: a functional genetic link for migraine? *J. Neurosci.* **22**, RC213 (2002).